

Low-lying electronic states of rhodium monocarbide and iridium monocarbide

Yubing Ren(任宇冰), Kaijie Zhang(张凯杰), Bing Yan(闫冰), and Wenli Zou(邹文利)
Citation: Chin. Phys. B, 2026, 35 (**8**): 083101. DOI: 10.1088/1674-1056/ae12df
http://cpb.iphy.ac.cn; http://iopscience.iop.org/cpb

What follows is a list of articles you may be interested in

Spectroscopic and transition properties of strontium chloride

Dong-Lan Wu(伍冬兰), Bi-Kun Liu(刘必坤), Wen-Tao Zhou(周文涛), Jia-Yun Chen(陈佳运), Zhang-Li Lai(赖章丽), Bo Liu(刘波), and Bing Yan(闫冰)
Chin. Phys. B, 2025, 34 (**4**): 043101. DOI: 10.1088/1674-1056/adb264

Spectroscopy and molecule opacity investigation on excited states of SiS

Rui Li(李瑞), Haonan Lv(吕浩男), Jiqun Sang(桑纪群), Xiaohua Liu(刘晓华), Guiying Liang(梁桂颖), and Yong Wu(吴勇)
Chin. Phys. B, 2024, 33 (**5**): 053101. DOI: 10.1088/1674-1056/ad20dc

Low-lying electronic states of osmium monoxide OsO

Wen Yan(严汶) and Wenli Zou(邹文利)
Chin. Phys. B, 2023, 32 (**11**): 113101. DOI: 10.1088/1674-1056/acec46

Relativistic calculations on the transition electric dipole moments and radiative lifetimes of the spin-forbidden transitions in the antimony hydride molecule

Yong Liu(刘勇), Lu-Lu Li(李露露), Li-Dan Xiao(肖利丹), and Bing Yan(闫冰)
Chin. Phys. B, 2022, 31 (**8**): 083101. DOI: 10.1088/1674-1056/ac6ee1

Theoretical study on the transition properties of AlF

Yun-Guang Zhang(张云光), Ling-Ling Ji(吉玲玲), Ru Cai(蔡茹),Cong-Ying Zhang(张聪颖), and Jian-Gang Xu(徐建刚)
Chin. Phys. B, 2022, 31 (**5**): 053101. DOI: 10.1088/1674-1056/ac3648

Low-lying electronic states of rhodium monocarbide and iridium monocarbide

Yubing Ren(任宇冰)[1,2], Kaijie Zhang(张凯杰)[1,2], Bing Yan(闫冰)[3,†], and Wenli Zou(邹文利)[1,2,‡]

[1] *Institute of Modern Physics, Northwest University, Xi'an* 710127, *China*
[2] *Shaanxi Key Laboratory for Theoretical Physics Frontiers, Xi'an* 710127, *China*
[3] *Institute of Atomic and Molecular Physics, Jilin University, Changchun* 130012, *China*

(Received 11 September 2025; revised manuscript received 10 October 2025; accepted manuscript online 14 October 2025)

This article presents a theoretical exploration of the electronic spectra of two cobalt group monocarbide molecules, RhC and IrC, utilizing the complete active space second-order perturbation theory (CASPT2) method. It encompasses all the low-lying Λ–S and Ω states below 4 eV (approximately 32000 cm^{-1}). The theoretical findings corroborate the previously established ground states: the $X^2\Sigma^+_{1/2}$ state for RhC and the $X_1{}^2\Delta_{5/2}$ state for IrC, alongside the closely lying first excited state $X_2{}^2\Sigma^+_{1/2}$. Additionally, a couple of excited states observed experimentally have been reasonably assigned based on these theoretical results, and the derived spectroscopic constants and radiative lifetimes (for RhC only) are generally consistent with available experimental data. These theoretical insights not only deepen our understanding of the electronic structures of RhC and IrC but also lay the groundwork for subsequent spectroscopic research on these two molecules.

Keywords: transition dipole moment, multi-reference second-order perturbation theory, spin–orbit coupling, exact two-component relativity, radiative lifetime

PACS: 31.15.A–, 31.15.aj, 31.15.am, 36.20.Kd

DOI: 10.1088/1674-1056/ae12df **CSTR:** 32038.14.CPB.ae12df

1. Introduction

Transition metal carbides are known for their exceptional hardness and high melting points.[1,2] Among the carbides of cobalt group elements, rhodium carbide (RhC) and iridium carbide (IrC) have yet to be synthesized in the lab, but theoretical predictions suggest intriguing properties. For instance, the carburization of face-centered cubic Rh could produce a remarkable metallization effect,[3] while zinc blende structured IrC is anticipated to be a conductive and ductile hard material.[4] As the simplest entities, diatomic gas-phase RhC and IrC molecules may provide insights into the chemical bonding interactions between transition metals and carbon atoms during physical and chemical processes. Despite some spectroscopic investigations on RhC[5–12] and IrC,[13–17] our understanding of their electronic structures remains quite limited.

In the 1960s, Scullman's research group conducted pioneering spectroscopic studies on the RhC molecule.[5,6,8] They identified the $X^2\Sigma \rightarrow A^2\Sigma$ and $X^2\Sigma \rightarrow B^2\Sigma$ transitions within the 400–500 nm absorption spectra.[5] Following the discovery of a new transition, $X^2\Sigma \rightarrow A^2\Pi$, in subsequent investigations, they renamed the earlier two transitions as $X^2\Sigma \rightarrow B^2\Sigma$ and $X^2\Sigma \rightarrow C^2\Sigma$, respectively.[6] Their findings indicated that the $B^2\Sigma$ and $C^2\Sigma$ states significantly perturb each other, and the $C^2\Sigma$ state is additionally affected by an unidentified D state exhibiting opposite $+/-$ symmetry. In 1969, they reported on the $X^2\Sigma \rightarrow A^2\Pi$ transition evident in both absorption and emission spectra ranging from 660 nm to 1225 nm, and successfully measured the spectroscopic constants of the two sub-states with $\Omega = 3/2$ and 1/2 of the $A^2\Pi$ state.[8] In 1972, Brom and colleagues[9] conducted an electron spin resonance (ESR) and optical spectroscopic study of RhC in neon and argon matrices at a temperature of 4 K. Through their analysis of the ESR spectrum, they deduced the electronic configuration of RhC, establishing its ground state as $X^2\Sigma^+$. Their examination of the absorption spectrum, spanning 350 nm to 1050 nm, revealed several transitions from the $X^2\Sigma^+$ ground state to the $A^2\Pi_{3/2,1/2}$, $B^2\Sigma^+$ and $C^2\Sigma^+$ states, including the identification of two new $^2\Sigma^+$ states. In 1998, Li and Wang[10] conducted an experimental study on RhC, along with RhN and RhO, utilizing anion photoelectron spectroscopy. They successfully identified the $X^2\Sigma^+$, $A^2\Pi_{3/2}$ and $A^2\Pi_{1/2}$ states. One year later, in 1999, Balfour *et al.*[11] employed a time-filtered laser-induced fluorescence (LIF) technique to measure the absorption and emission spectra of RhC in the range of 400–500 nm. Their findings confirmed that the previously identified $B^2\Sigma^+$ and $D^2\Sigma^-$ states are actually sub-states of a $^2\Pi$ state, leading them to rename these states as $D^2\Pi_{3/2}$ and $D^2\Pi_{1/2}$, respectively; they proceeded to measure their radiative lifetimes. In 2012, Gong *et al.*[12] examined the infrared

†Corresponding author. E-mail: yanbing@jlu.edu.cn
‡Corresponding author. E-mail: zouwl@nwu.edu.cn

© 2026 Chinese Physical Society and IOP Publishing Ltd. All rights, including for text and data mining, AI training, and similar technologies, are reserved.

spectra of RhC in neon and argon matrices.

The early spectroscopic studies of IrC were also conducted by Scullman's research group.[13,14] In 1969, they identified two transitions in the absorption and emission spectra within the range of 480–530 nm, corresponding to the upper states $^2\Pi_{3/2}$ and $^2\Phi_{7/2}$, with a common lower state of $^2\Delta_{5/2}$.[13] In a subsequent study in 1970, they observed multiple sets of transitions in the absorption and emission spectra between 660 nm and 850 nm, which were attributed to the transitions $E^2\Delta_{3/2} \rightarrow X^2\Delta_{3/2}$ and $X^2\Delta_{5/2} \leftrightarrow E^2\Delta_{5/2}$, $D^2\Phi_{7/2}$, $K^2\Pi_{3/2}$ and $L^2\Phi_{7/2}$.[14] In 1996, Marr *et al.*[15] investigated the hyperfine and Stark spectra of the $X^2\Delta_{5/2}$–$D^2\Phi_{7/2}$ system through LIF spectroscopy. They measured the dipole moments and the electric quadrupole hyperfine interactions of both states. Subsequently, in 2004, Cheung's research group examined the $X^2\Delta_{5/2} \rightarrow L^2\Phi_{7/2}$ absorption spectrum, resulting in the acquisition of high-precision spectroscopic constants for the upper state.[16] In 2009, they employed laser ablation/reaction free jet expansion and LIF spectroscopy to analyze the spectral band within the range of 394–520 nm.[17] Alongside the transitions from $X^2\Delta_{5/2}$ to $K^2\Pi_{3/2}$ and $L^2\Phi_{7/2}$, they also identified and assigned several new absorption transitions to the $[19.4]^2\Pi_{3/2}$, $[23.0]^2\Pi_{3/2}$ and two $\Omega = 3/2$ states.

In addition to the aforementioned spectroscopic studies, the dissociation energies[18–20] (refer to the citations in Ref. [21]) and the ionization potentials[21] for RhC and IrC were also determined. Notably, Huber and Herzberg compiled the early spectroscopic data for RhC and IrC prior to 1977 in their data book.[22]

In the existing literature, some theoretical studies have also been undertaken regarding RhC[12,20,21,23–31] and IrC.[20,21,30,32–34] However, these studies primarily focus on ground state calculations using spin-free density functional theory (DFT). Notable exceptions include the research conducted by Shim and Gingerich[23] and Balasubramanian's group,[25,32] who examined the low-lying electronic states of RhC and IrC in the last century. They employed single-reference configuration interaction and multi-reference configuration interaction (MRCI) methods, respectively. It is worth noting that the effects of spin–orbit coupling (SOC) were only considered for the experimentally observed seven Ω states of IrC.[32]

In this article, we comprehensively investigate the low-lying Λ–S and Ω electronic states of RhC and IrC, delving into their spectroscopic properties.

2. Theoretical method

Scalar relativistic effects are integrated using the spin-free exact two-component (sf-X2C) Hamiltonian,[35,36] which takes into account the finite size of the nuclear charge distribution. The basis set utilized for carbon, rhodium and iridium is ANO-R3,[37,38] featuring a 4-ζ quality. All the low-lying doublet and quartet Λ–S states of RhC and IrC below 32000 cm^{-1} have been calculated using the quadratically convergent SA-CASSCF (state-averaged complete active space self-consistent field) method. This approach maintains adherence to C_{2v} point group symmetry and incorporates additional constraints related to linear molecular supersymmetry. For RhC, two additional states, $[1]^4\Sigma^-$ and $[3]^4\Delta$, are also computed as their excitation energies are very close to the upper limit. Although sextet states were also investigated, they were found to have energies exceeding 35000 cm^{-1}, as indicated by Balasubramanian *et al.*,[25,32] and are therefore not reported in this study. Notably, their computed $^6\Sigma^+$ state of IrC, positioned around 30000 cm^{-1},[32] could not be obtained in this study and was therefore excluded from the final calculations. In the literature on multi-reference calculations of RhC and IrC, an active space of (13e,10o) is commonly employed,[25,31–33] which accounts for all 13 valence electrons across 10 valence molecular orbitals derived from the C 2s2p and Rh 4d5s (or Ir 5d6s) shells. However, in this study, we propose an expanded active space of (13e,13o) by incorporating an additional p′ shell comprising C 3s3p and Rh 5p or Ir 6p. This adjustment allows us to account for possible excitations to the Rh 5p or Ir 6p orbitals, as previously noted in the calculations regarding IrC performed by Balasubramanian *et al.*[32]

In the subsequent computations involving dynamic correlation processing, we utilize CASPT2 (complete active space second-order perturbation theory).[39,40] This approach accounts for 13 valence electrons, along with the correlations of eight semi-core electrons from Rh 4s4p, as well as 22 semi-core electrons from Ir 4f5s5p. To address the common intruder state issues in CASPT2, we apply both an IPEA shift[41] of 0.25 a.u. and a σ^2-regularization[42] of 0.25 a.u. simultaneously, ensuring that the weights of reference configurations remain at 84% or higher. Following this, we construct a second-order effective Hamiltonian for the selected roots with the same quantum numbers Λ and S. After diagonalization, we obtain the final energies from the RMS-CASPT2 (rotated multi-state CASPT2) procedure[43] and the perturbatively modified (PM) CASSCF wavefunctions.

The SOC effects are addressed through the state-interaction (SI) procedure.[44] In this method, the spin–orbit matrix is constructed using the PM-CASSCF wavefunctions derived from the RMS-CASPT2 calculations. Furthermore, two-electron spin–orbit integrals are calculated employing the atomic mean field integral approximation,[45] while the diagonal elements of the spin–orbit matrix are replaced with the corresponding RMS-CASPT2 energies.

The SA-CASSCF method is integrated in the BDF quantum chemistry software package.[46] For the execution of

CASCI (complete active space configuration interaction using the CIONLY keyword in the RASSCF module), RMS-CASPT2 and SI calculations, we employ the OpenMolcas software package.[47,48] The interface connecting BDF and OpenMolcas is established through SA-CASSCF wavefunctions, with comprehensive details available in our recent publication.[49] Spectroscopic constants are obtained by numerically solving the one-dimensional Schrödinger equation with Le Roy's Level program,[50] which provides the adiabatic excitation energy (T_e), equilibrium bond length (R_e), vibrational frequency (ω_e) and rotational constant (B_e). Additionally, the Multiwfn[51,52] and NBO[53] programs are utilized for analyzing the wavefunctions produced in the CASCI calculations.

3. Results and discussion

3.1. Low-lying Λ–S states of RhC

The potential energy curves (PECs) for the low-lying Λ–S states of the RhC molecule below 32000 cm^{-1} are illustrated in Fig. 1. The fitted spectroscopic constants, along with the dominant configurations, are compiled in Table 1. Additionally, Table 2 presents the bond orders and natural atomic configurations for these Λ–S states.

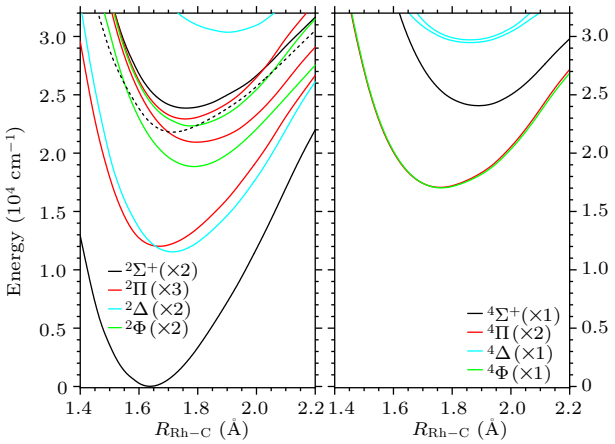


Fig. 1. PECs of low-lying Λ–S states of RhC. The dashed line is the PEC of $[2]^2\Sigma^+$ calculated using the AVQZ basis set.

Table 1. Spectroscopic constants of Λ–S states of ^{103}Rh^{12}C.

Λ–S state	T_e (cm^{-1})	R_e Å	ω_e (cm^{-1})	B_e (cm^{-1})	Dominant configurations at R_es $1\sigma/2\sigma/3\sigma/4\sigma/1\pi/2\pi/1\delta$ ($\geq$ 10%)[a]
$[1]^2\Sigma^+$	0	1.636	1016	0.5859	2210404 (73) + 2210314 (11)
Expt.[b]	0	1.613	1050	0.6027	
$[2]^2\Sigma^+$	23851	1.761	678	0.5002	2210314 (37) + 2201404 (17) + 2120404 (12)
$[2]^2\Sigma^+$[c]	21785	1.715	861	0.5336	2201404 (81)
Expt.[b]	21439	1.687	928	0.5510	
Expt.[d]	20937	1.681	911	0.5554	
$[1]^2\Pi$	12009	1.668	878	0.5557	2200414 (74)
$[2]^2\Pi$	20928	1.797	678	0.4777	2210413 (77)
$[3]^2\Pi$	22921	1.758	766	0.5005	2210413 (74)
$[1]^2\Delta$	11530	1.714	904	0.5305	2220403 (74)
$[2]^2\Delta$	30303	1.904	762	0.4378	2200423 (67) + 2110423 (12)
$[1]^2\Phi$	18843	1.789	766	0.4885	2210413 (78)
$[2]^2\Phi$	22320	1.776	776	0.4908	2210413 (77)
$[1]^4\Sigma^+$	23927	1.898	862	0.4437	2210314 (69)
$[1]^4\Sigma^-$	32370	1.928	668	0.4219	2210314 (61) + 2220313 (12)
$[1]^4\Pi$	17059	1.759	742	0.5006	2210413 (84)
$[1]^4\Delta$	29464	1.865	522	0.4526	2200423 (69) + 2110423 (15)
$[2]^4\Delta$	29700	1.862	540	0.4536	2210314 (62) + 2211403 (13)
$[3]^4\Delta$	32167	1.840	644	0.4632	2211403 (33) + 2220313 (28) + 2210314 (15)
$[1]^4\Phi$	17021	1.763	735	0.4978	2210413 (83)

[a] Computed at the PM-CASSCF level. 1σ & 2σ: C 2s + Rh 4d$_\sigma$, 3σ & 4σ: C 2p$_\sigma$ + Rh 5s, 1π & 2π: C 2p$_\pi$ + Rh 4d$_\pi$, and 1δ: Rh 4d$_\delta$. The higher-lying three auxiliary active orbitals 5σ and 3π are always weakly occupied.
[b] Ref. [22]. [c] Calculated using the AVQZ basis set. [d] Deperturbed results from Ref. [11].

The theoretical findings suggest that the ground state of RhC is $[1]^2\Sigma^+$ (also known as $X^2\Sigma^+$), which aligns with the findings for CoC[54] and matches the experimental results[22] as well as the theoretical predictions made by Balasubramanian *et al.*[25] The calculated bond length and vibrational frequency are found to be 1.636 Å and 1016 cm^{-1}, respectively, compared with the experimental values of 1.613 Å and 1050 cm^{-1}. These discrepancies are considered acceptable, especially since the current theoretical calculations do not account for SOC effects. Notably, the MRCI-derived bond length of 1.552 Å reported by Balasubramanian *et al.*[25] is considerably shorter, likely due to limitations in the size of their basis set and the absence of core–valence correlations in their computations. Our findings indicate that the electronic configuration $1\sigma^2 2\sigma^2 3\sigma^1 1\pi^4 1\delta^4$ constitutes 73% of the ground state, aligning qualitatively with the weight of 83%

reported in the literature.[25] Moreover, a secondary configuration, $1\sigma^2 2\sigma^2 3\sigma^1 1\pi^3 2\pi^1 1\delta^4$, accounts for an additional 11%. This suggests that while the ground state is predominantly influenced by a single configuration, it also exhibits some multi-configuration characteristics.

In transition metal carbides, carbon atoms display a diverse range of bonding characteristics. The literature suggests that in its ground state the RhC molecule possesses a Rh≡C triple bond.[23–25] However, the effective bond order (EBO) derived from the dominant configuration is only 2.5. In the strongly occupied active orbitals, the bonding characteristics are as follows: 2σ, 3σ and 1π are classified as bonding orbitals, while 1σ is an anti-bonding orbital and 1δ is a non-bonding orbital. Thus, the calculation for EBO yields $(2+1+4-2)/2 = 2.5$. This finding is corroborated by additional methods; for instance, Mayer's bond order (MBO) is measured at 2.28 and the Wiberg bond index (WBI) utilizing natural atomic orbitals is 2.13, indicating it is roughly half a bond lower than the previously estimated triple bond. The NBO analysis indicates that the natural atomic configurations of the two atoms in the $X^2\Sigma^+$ state are Rh $5s^{0.89}4d^{8.08}5p^{0.04}$ and C $2s^{1.85}2p^{2.08}$, respectively. This suggests that both Rh and C are situated in their respective atomic ground states, ^{4}F and ^{3}P,[55] with minimal charge transfer occurring between them. Consequently, the bond order of 2.5 is predominantly a result of polarized covalent interactions.

All low-lying Λ–S excited states of RhC are situated above 10000 cm^{-1}, as illustrated in Fig. 1. In contrast to many diatomic transition metal radicals, the distribution of these excited states is notably sparse. For these states, only the $[1]^2\Pi$ and $[1]^2\Delta$ states exhibit bond orders that are comparable to that of the ground state, while the bond orders of the other states diminish by 0.5–1.0, as detailed in Table 2. Moreover, in most of these excited states, the Rh atom approximately retains a ground-state configuration of $5s^14d^8$ (^{4}F), which is similar to the ground state configuration. However, for the $[1]^2\Pi$, $[2]^2\Delta$, and $[1]^4\Delta$ states, the Rh atom configurations are significantly closer to $5s^04d^8$, with the occupation numbers of the C 2p shell ranging from 2.4 to 2.7. This indicates a higher presence of ionic bond characteristics within their Rh–C bonds, represented as Rh^+C^-. It is important to highlight that the natural atomic configurations of Rh in several states show notable occupations in the 5p shell, often reaching or even surpassing 0.2. The comparison of RMS-CASPT2 results with and without the inclusion of the p′ active orbitals reveals that the vertical energy differences at 1.62 Å are typically less than 0.1 eV. However, for the $[2]^2\Delta$ and $[1]^4\Delta$ states, which exhibit an occupation number of approximately 0.25 in the Rh 5p orbitals as indicated in Table 2, the differences rise to 0.15 eV. This finding highlights the importance of incorporating the p′ shell into the active space.

Table 2. Bond orders and natural atomic configurations for Λ–S states of RhC at 1.62 Å.

Λ–S state	MBO	WBI	Atomic config. (Rh)	Atomic config. (C)
$[1]^2\Sigma^+$	2.28	2.13	$5s^{0.89}4d^{8.08}5p^{0.04}$	$2s^{1.85}2p^{2.08}$
$[2]^2\Sigma^+$	1.75	1.66	$5s^{1.09}4d^{7.86}5p^{0.06}$	$2s^{1.61}2p^{2.30}$
$[1]^2\Pi$	2.03	1.79	$5s^{0.12}4d^{8.31}5p^{0.18}$	$2s^{1.87}2p^{2.44}3p^{0.06}$
$[2]^2\Pi$	1.62	1.41	$5s^{0.91}4d^{7.76}5p^{0.11}$	$2s^{1.82}2p^{2.33}$
$[3]^2\Pi$	1.60	1.40	$5s^{0.83}4d^{7.81}5p^{0.08}$	$2s^{1.85}2p^{2.36}$
$[1]^2\Delta$	2.23	1.97	$5s^{1.46}4d^{7.56}5p^{0.06}$	$2s^{1.85}2p^{2.00}$
$[2]^2\Delta$	1.53	1.20	$5s^{0.14}4d^{8.00}5p^{0.24}$	$2s^{1.84}2p^{2.69}3p^{0.07}$
$[1]^2\Phi$	1.62	1.41	$5s^{0.90}4d^{7.75}5p^{0.11}$	$2s^{1.83}2p^{2.34}$
$[2]^2\Phi$	1.59	1.39	$5s^{0.89}4d^{7.75}5p^{0.08}$	$2s^{1.84}2p^{2.36}$
$[1]^4\Sigma^+$	1.24	1.09	$5s^{0.86}4d^{7.79}5p^{0.09}$	$2s^{1.85}2p^{2.35}$
$[1]^4\Sigma^-$	1.27	1.10	$5s^{0.85}4d^{7.76}5p^{0.12}$	$2s^{1.83}2p^{2.39}$
$[1]^4\Pi$	1.69	1.48	$5s^{0.87}4d^{7.73}5p^{0.13}$	$2s^{1.84}2p^{2.35}$
$[1]^4\Delta$	1.60	1.25	$5s^{0.13}4d^{7.96}5p^{0.25}$	$2s^{1.84}2p^{2.71}3p^{0.07}$
$[2]^4\Delta$	1.51	1.35	$5s^{0.98}4d^{7.69}5p^{0.08}$	$2s^{1.87}2p^{2.24}3s^{0.09}$
$[3]^4\Delta$	1.27	1.12	$5s^{0.90}4d^{7.74}5p^{0.11}$	$2s^{1.86}2p^{2.31}$
$[1]^4\Phi$	1.68	1.46	$5s^{0.87}4d^{7.73}5p^{0.12}$	$2s^{1.84}2p^{2.36}$

The lack of SOC effects leaves the relationship between most calculated Λ–S states and those observed experimentally unclear. In this discussion, we focus specifically on the $C^2\Sigma^+$ excited state, which has also been referred to as $E^2\Sigma^+$ by Balasubramanian *et al.*[25] and Balfour *et al.*,[11] and is located around 21000 cm^{-1}. Due to no first-order SOC, this state can be reasonably assigned to the calculated $[2]^2\Sigma^+$ state. However, it is noteworthy that the predicted excitation energy is approximately 2500 cm^{-1} higher than what is experimentally observed, surpassing the typical accuracy limit of 0.2 eV (about 1600 cm^{-1}) associated with the CASPT2 methodology. Even when accounting for second-order SOC effects, improvements to the energy of the $[2]^2\Sigma^+$ state remain elusive. The significant error may be attributed to the excessive contraction of p-functions in the ANO-R3 basis set of carbon, which we encountered in our recent theoretical study of the WN molecule.[56] To verify this, we recalculated the two states, $[1]^2\Sigma^+$ and $[2]^2\Sigma^+$, using the aug-cc-pwCVQZ-PP[57] and aug-cc-pVQZ[58] basis sets (referred to as AVQZ) for Rh and C, respectively. In this context, the innermost 28 core electrons of Rh are replaced by relativistic pseudo-potentials.[57] After switching to the AVQZ basis set, the excitation energy of $[2]^2\Sigma^+$ decreased from 23851 cm^{-1} to 21785 cm^{-1}. Additionally, the bond length was shortened from 1.761 Å to 1.715 Å, and the vibrational frequency increased from 678 cm^{-1} to 861 cm^{-1}, aligning more closely with experimental values. Furthermore, there are also changes in the dominant configuration (refer to Table 1) and the natural atomic configuration (see Table 2).

3.2. Low-lying Ω states of RhC

After evaluating the SOC effects using the SI approach, the Λ–S states split into Ω states. Figure 2 displays the PECs of all Ω states below 32000 cm^{-1}, which include ten

states with $\Omega = 1/2$, ten states with $\Omega = 3/2$, seven states with $\Omega = 5/2$, five states with $\Omega = 7/2$, and one state with $\Omega = 9/2$. Due to an insufficient number of higher-lying auxiliary Λ–S states in the spin–orbit matrix, the results for Ω states above 32000 cm^{-1} are deemed unreliable and are therefore excluded. The spectroscopic constants for these Ω states are summarized in Table 3, where they are compared against the experimental values. Additionally, the squared total transition dipole moments ($|\mu|^2$) between the ground state and the excited Ω state at a bond length of 1.62 Å are presented in the table. It is important to note that in the RMS-CASPT2/SI calculations, the energy of the $[2]^2\Sigma^+$ state is overestimated due to the defect of the basis set and is subsequently adjusted down by 2066 cm^{-1} to accurately reflect the observed spectral transitions.

The PECs presented in Fig. 2 reveal a substantial energy gap exceeding 10000 cm^{-1} between the ground and excited Ω states of RhC. This considerable separation diminishes uncertainties when identifying the spectral bands associated with transitions between electronic states. Indeed, in all observed absorption and emission transitions of RhC, the lower state has been consistently identified as the ground state. In the following section, we will delve deeper into these Ω states and discuss their correlation with the electronic states assigned based on experimental observations.

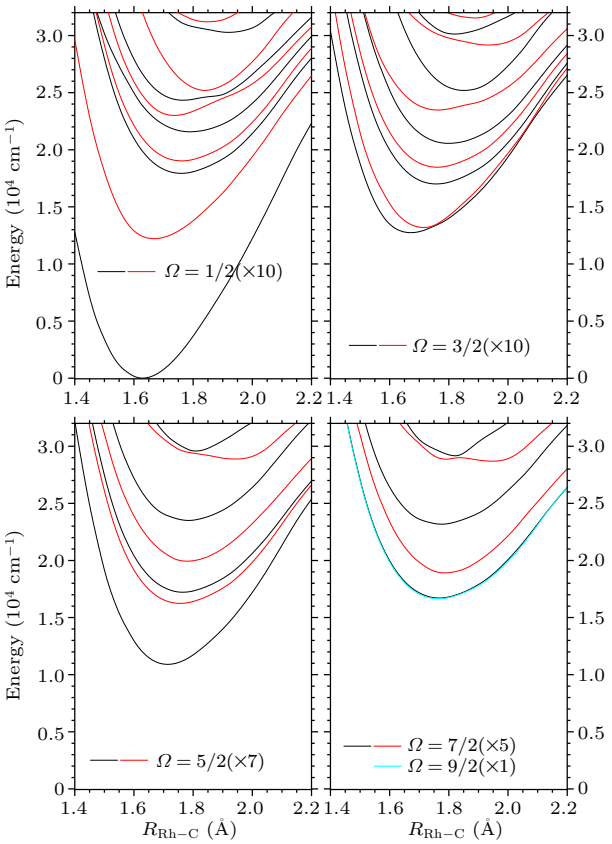


Fig. 2. PECs of low-lying Ω states of RhC.

Table 3. Spectroscopic constants of Ω states of $^{103}Rh^{12}C$.[a)]

Ω state	T_e (cm^{-1})	R_e (Å)	ω_e (cm^{-1})	B_e (cm^{-1})	$\lvert\mu^2\rvert$ to $\{1\}1/2$[b)] (a.u.)	Components[b)] ($\geq$ 10%)
$\{1\}1/2$	0	1.629	1054	0.5892		$[1]^2\Sigma^+$ (99)
Expt.	0	1.613	1050	0.6027		$X^2\Sigma^+$
$\{2\}1/2$	12165	1.667	878	0.5563	0.3272	$[1]^2\Pi$ (99)
Expt.	9463	1.655	949	0.5733		$A^2\Pi_{1/2}$ [c)]
$\{3\}1/2$	17885	1.760	743	0.5004	0.0034	$[1]^4\Pi$ (97)
$\{4\}1/2$	18981	1.762	739	0.4989	0.0151	$[1]^4\Pi$ (99)
$\{5\}1/2$	21574	1.791	650	0.4842	1.1172	$[2]^2\Sigma^+$ (81) + $[2]^2\Pi$ (17)
Expt.	21439	1.687	928	0.5510		$C^2\Sigma^+$
Expt.	20937	1.681	911	0.5554		$C^2\Sigma^+$ (aka $E^2\Sigma^+$) [d)]
$\{6\}1/2$	23005	1.735	832	0.5112	0.3238	$[2]^2\Pi$ (72) + $[2]^2\Sigma^+$ (16)
Expt.	[21291]	1.772	[816]	0.4996		$D^2\Pi_{1/2}$ (aka $B^2\Pi_{1/2}$) [e)]
$\{7\}1/2$	24339	1.766	735	0.4730	0.0260	$[3]^2\Pi$ (89)
Expt.	[22516]		[706]			$U_2{}^2\Sigma^+$ ($U_2{}^2\Pi_{1/2}$ in this work) in Ne matrix [f)]
$\{8\}1/2$	25159	1.839	955	0.4602	0.0004	$[1]^4\Sigma^+$ (99)
$\{9\}1/2$	30193	1.917	645	0.4415		$[1]^4\Delta$ (99)
$\{10\}1/2$	31157	1.839	690	0.4638	0.0003	$[2]^4\Delta$ (99)
$\{1\}3/2$	12745	1.671	866	0.5500	0.3102	$[1]^2\Pi$ (99)
Expt.	10243	1.655	939	0.5715		$A^2\Pi_{3/2}$ [g)]
$\{2\}3/2$	13200	1.715	934	0.5350		$[1]^2\Delta$ (99)
$\{3\}3/2$	17011	1.757	747	0.5018	0.0002	$[1]^4\Pi$ (98)
$\{4\}3/2$	18478	1.761	738	0.4991		$[1]^4\Phi$ (99)
$\{5\}3/2$	20564	1.799	677	0.4793	0.1176	$[2]^2\Pi$ (80) + $[3]^2\Pi$ (19)
Expt.	[21361]	[1.760]		[0.5067]		
Expt.	20990	1.757	753	0.5084		$D^2\Pi_{3/2}$ (aka $B^2\Pi_{3/2}$) [d)]
$\{6\}3/2$	23487	1.762	707	0.4822	0.0244	$[3]^2\Pi$ (79) + $[2]^2\Pi$ (19)
Expt.	[22280]					$U_1{}^2\Sigma^+$ in Ne matrix with an unknown ν' [f)]
Expt.	[22613]	[1.760]	[789]	[0.5067]		$U_3{}^2\Pi_{3/2}$ [e)]

Table 3. (*Continued*).

Ω state	T_e (cm^{-1})	R_e (Å)	ω_e (cm^{-1})	B_e (cm^{-1})	$\lvert\mu^2\rvert$ to {1}1/2[b)] (a.u.)	Components[b)] ($\geq$ 10%)
{7}3/2	25178	1.851	758	0.4578	0.0012	$[1]^4\Sigma^+$ (98)
{8}3/2	29156	1.926	597	0.4361		$[1]^4\Delta$ (84) + $[2]^2\Delta$ (16)
{9}3/2	30139	1.833	718	0.4671	0.0001	$[2]^4\Delta$ (95)
{10}3/2	31570	1.871	654	0.4482		$[2]^2\Delta$ (81) + $[1]^4\Delta$ (14)
{1}5/2	10908	1.714	903	0.5305		$[1]^2\Delta$ (99)
{2}5/2	16249	1.756	748	0.5026		$[1]^4\Pi$ (99)
{3}5/2	17225	1.764	755	0.4976		$[1]^4\Phi$ (84) + $[1]^2\Phi$ (14)
{4}5/2	19942	1.780	775	0.4885		$[1]^2\Phi$ (80) + $[1]^4\Phi$ (15)
{5}5/2	23506	1.784	738	0.4905		$[2]^2\Phi$ (94)
{6}5/2	28873	1.940	578	0.4433		$[1]^4\Delta$ (92)
{7}5/2	29544	1.810	1043	0.4756		$[2]^4\Delta$ (99)
{1}7/2	16715	1.766	750	0.4966		$[1]^4\Phi$ (89) + $[1]^2\Phi$ (11)
{2}7/2	18917	1.788	777	0.4859		$[1]^2\Phi$ (79) + $[2]^2\Phi$ (11) + $[1]^4\Phi$ (10)
{3}7/2	23179	1.776	724	0.4948		$[2]^2\Phi$ (89)
{4}7/2	28689	1.952	654	0.4656		$[1]^4\Delta$ (99)
{5}7/2	29096	1.825	1222	0.4926		$[2]^4\Delta$ (99)
{1}9/2	16656	1.764	735	0.4969		$[1]^4\Phi$ (100)

[a)]Experimental spectroscopic constants are taken from Ref. [22] by default. The values in brackets are T_0, R_0, $\Delta G_{1/2}$ and B_0. State U_n means the nth unrecognized state in the literature.
[b)]Computed at 1.62 Å. [c)]$A^2\Pi_{3/2}$ by mistake in Ref. [9]. [d)]Deperturbed results from Ref. [11]. [e)]Ref. [11]. [f)]Ref. [9]. [g)]$A^2\Pi_{1/2}$ by mistake in Ref. [9].

The ground state X1/2 (or {1}1/2) from $X^2\Sigma^+$ The ground Ω state of RhC, denoted as {1}1/2 or X1/2, is primarily derived from the ground Λ–S state $[1]^2\Sigma^+$, with a significant contribution of 99%. When compared with the parent state $[1]^2\Sigma^+$, the bond length of {1}1/2 has decreased from 1.636 Å to 1.629 Å, while the vibrational frequency has risen from 1016 cm^{-1} to 1054 cm^{-1}, approaching the experimental values of 1.613 Å and 1050 cm^{-1}.

The $\Omega = 1/2$ and 3/2 states from $A^2\Pi$ There is some confusion in the literature regarding the naming of the $A^2\Pi$ state. Some authors have renamed it the $B^2\Pi$ state due to the presence of a quasi-degenerate $[1]^2\Delta$ state.[11,25] However, since $[1]^2\Delta$ is a dark state, and considering that the $D^2\Pi$ state (see later) has also been referred to as $B^2\Pi$,[11] we choose to maintain the designation $A^2\Pi$ in this study. The $A^2\Pi$ state was experimentally detected relatively early in both absorption[8,9] and emission spectra,[8] revealing two Ω components: $A^2\Pi_{1/2}$ with lower energy and $A^2\Pi_{3/2}$ with higher energy. These components may correspond to our calculated states {2}1/2 and {1}3/2, which originate from the $[1]^2\Pi$ state. It should be highlighted that Table I in Ref. [9] contains a labeling error for the $A^2\Pi_{1/2}$ and $A^2\Pi_{3/2}$ states (these states are accurately labeled in the other tables and figures within the same reference), and this mistake also appears in Table IV of Ref. [9]. The excitation energies for these two states exceed the experimental values by 2700 cm^{-1} and 2500 cm^{-1}, which seems somewhat excessive and may again stem from the basis set issue observed earlier with the $C^2\Sigma^+$ state. The energy difference between these two states, known as the SOC splitting energy, is 580 cm^{-1}, which is 200 cm^{-1} less than the experimental value of 780 cm^{-1}. Their bond lengths are approximately 1.67 Å, which is close to the experimental measurement of 1.655 Å, while their vibrational frequencies are around 870 cm^{-1}, which qualitatively align with the experimental values of approximately 940 cm^{-1}.

The $\Omega = 1/2$ state from $C^2\Sigma^+$ It is proposed to rename the $C^2\Sigma^+$ state as the $E^2\Sigma^+$ state due to the existence of a $[1]^2\Phi$ state with slightly lower energy[11,25] (see Table 1). Based on the predominant Λ–S state component, the $C^2\Sigma^+$ state aligns with our calculated {5}1/2 state, which primarily originates from the $[2]^2\Sigma^+$ state, accounting for 81% of its character, but also incorporates 17% from the $[2]^2\Pi$ component. The modification of the $[2]^2\Sigma^+$ state energy in the SI calculations results in the {5}1/2 excitation energy of 21574 cm^{-1} being quite close to the experimental value of 21439 cm^{-1} [22] and the deperturbed value of 20937 cm^{-1}.[11] Nevertheless, the shape of the PEC for the $[2]^2\Sigma^+$ state calculated using the ANO-R3 basis set is also inaccurate (refer to Fig. 1), leading to significant discrepancies in the bond length and vibrational frequency of the {5}1/2 state.

The $\Omega = 1/2$ and 3/2 states from $D^2\Pi$ The nomenclature of the $D^2\Pi$ system in the literature can be perplexing for readers. The branches with lower $\Omega = 3/2$ and higher $\Omega = 1/2$ have been respectively referred to as $B^2\Sigma$ (originally labeled as the $A^2\Sigma$ state[5]) and $D^2\Sigma$ states,[6] which were later designated as $B^2\Sigma^+$ and $D^2\Sigma^-$ states.[9,22] In 1999, it was determined that they correspond to the two Ω components of a $^2\Pi$ state, specifically termed $D^2\Pi_{3/2}$ and $D^2\Pi_{1/2}$ states.[11] However, the same paper also simultaneously employed the aliases $B^2\Pi_{3/2}$ and $B^2\Pi_{1/2}$, along with suggesting $B^2\Pi$ as an alias for the lower $A^2\Pi$ state (as mentioned above). To prevent confusion, we will consistently use the designation $D^2\Pi$ for the parent state throughout this paper, clarifying that there is no $B^2\Pi$ state within our naming framework.

In the experiments, the energies of the $D^2\Pi_{3/2}$ and $D^2\Pi_{1/2}$ states, along with the previously mentioned $C^2\Sigma^+$ states, are closely aligned, resulting in a complex perturbed system.[11] The $D^2\Pi_{3/2}$ and $D^2\Pi_{1/2}$ states can be classified into the $\{5\}3/2$ and $\{6\}1/2$ categories based on our calculations. Both states exhibit dominant characteristics of $[2]^2\Pi$ with an approximately 80% contribution, although they also incorporate a minor amount of $[3]^2\Pi$ and $[2]^2\Sigma^+$, respectively. The excitation energy for the $\{5\}3/2$ state, measured at 20564 cm^{-1}, closely matches the deperturbed experimental value of 20990 cm^{-1}.[11] Conversely, the excitation energy for the $\{6\}1/2$ state, recorded at 23005 cm^{-1}, is noticeably higher than the experimental value of around 21300 cm^{-1}.[11] This discrepancy highlights the need for a detailed deperturbation analysis of the $D^2\Pi_{1/2}$ state in forthcoming experiments. The bond lengths and vibrational frequencies of the $\{5\}3/2$ and $\{6\}1/2$ states exhibit significant differences when compared with experimental values. This discrepancy may once more be linked to the imprecise PEC shape of $[2]^2\Pi$ derived from calculations using the ANO-R3 basis set.

Other excited states in experiments In a Ne matrix at 4 K, two sets of absorption bands were identified at approximately 444.0 nm and between 417.3 nm and 448.7 nm. These bands are believed to represent transitions from the ground state to two distinct excited $^2\Sigma^+$ states,[9] which we refer to as the lower $U_1{}^2\Sigma^+$ and the higher $U_2{}^2\Sigma^+$ states for ease of discussion. In 1999, Balfour *et al.*[11] recorded three very weak absorption bands at 442.22 nm, 427.32 nm and 413.90 nm, which were proposed to arise from the transition $X1/2 \rightarrow {}^2\Pi_{3/2}$. In this study we designate the upper state in this transition as $U_3{}^2\Pi_{3/2}$. According to the theoretical excitation energies and $|\mu|^2$ values, $U_1{}^2\Sigma^+$ and $U_3{}^2\Pi_{3/2}$ can both be classified under the $\{6\}3/2$ state, indicating they are part of the same Ω state. On the other hand, $U_2{}^2\Sigma^+$ corresponds solely to $\{7\}1/2$ and should therefore be relabeled as $U_2{}^2\Pi_{1/2}$. Both Ω states primarily originate from the parent state $[3]^2\Pi$, and the calculated bond lengths and vibrational frequencies align closely with the available experimental data.

Radiative lifetimes of excited states At this stage, all experimentally observed spectral bands have been successfully linked to transitions between the ground state and the theoretically identified excited states. Notably, every one of these transitions exhibits a substantial $|\mu|^2$ value greater than 0.02 a.u. (refer to Table 3). Furthermore, the $|\mu|^2$ value associated with the $\{4\}1/2$ state (predominantly derived from $[1]^4\Pi$) situated around 19000 cm^{-1} in relation to the ground state is roughly 0.015 a.u., suggesting that this transition has the potential to be detected in upcoming spectroscopic studies. Other absorption transitions appear to be either forbidden or characterized by relatively low $|\mu|^2$ values, indicating that the emergence of new absorption bands for the RhC molecule is improbable within the energy range of 32000 cm^{-1}.

Based on Eq. (7) in the supporting information of Ref. [59], the radiative lifetime of each bright excited Ω state at its $v' = 0$ vibrational level can be estimated using the $|\mu|^2$ data in conjunction with the vertical excitation energy. For the $A^2\Pi_{1/2}$ and $A^2\Pi_{3/2}$ states, the predicted radiative lifetimes are approximately 11 μs; however, no experimental values are currently available for comparison. In contrast, the calculated radiative lifetimes for the $C^2\Sigma^+$, $D^2\Pi_{1/2}$ and $D^2\Pi_{3/2}$ states are 96 ns, 316 ns and 908 ns, respectively, which show reasonable agreement with the experimental values of 80 ns, 100 ns and 800 ns.[11] For the $U_2{}^2\Pi_{1/2}$ state, we observe three emission transitions with moderate intensities: $U_2{}^2\Pi_{1/2} \rightarrow X1/2$, $A^2\Pi_{1/2}$ and $\{2\}3/2$ (originating from $[1]^2\Delta$). The corresponding radiative lifetimes are 101 μs, 67 μs and 7.2 μs, respectively, leading to a total radiative lifetime for $U_2{}^2\Pi_{1/2}$ of 6.1 μs. Similarly, the $U_3{}^2\Pi_{3/2}$ state features three moderately strong emission transitions: $U_3{}^2\Pi_{3/2} \rightarrow X1/2$, $A^2\Pi_{1/2}$ and $A^2\Pi_{3/2}$. The radiative lifetimes for these transitions are 128 μs, 467 μs and 307 μs, respectively, resulting in a total radiative lifetime of 75 μs for $U_3{}^2\Pi_{3/2}$. The experimental radiative lifetime of the $U_3{}^2\Pi_{3/2}$ state at the $v' = 2$ level has been measured to be 600±25 ns,[60] which is significantly shorter than our estimated lifetime. Generally, lifetime deviations exhibiting such qualitative inconsistency are caused by imprecise second-order SOC effects. It is important to note that the $\{6\}3/2$ state (i.e., the $U_3{}^2\Pi_{3/2}$ state) consists of a dominant component, $[3]^2\Pi$, and a secondary component, $[2]^2\Pi$. The relative weights of these components are highly sensitive to the theoretical energy gap between the two $^2\Pi$ states, particularly through second-order SOC effects, which are challenging to accurately calculate. When ignoring SOC, we observe that the transition $X^2\Sigma^+$–$[2]^2\Pi$ is allowed, while the transition $X^2\Sigma^+$–$[3]^2\Pi$ is quite weak. Consequently, a higher proportion of $[2]^2\Pi$ in the $\{6\}3/2$ state corresponds to a shorter lifetime for the $U_3{}^2\Pi_{3/2}$ state.

3.3. Low-lying Λ–S states of IrC

The PECs for the low-lying Λ–S states of IrC, situated below 32000 cm^{-1}, are illustrated in Fig. 3. Table 4 provides a summary of the associated spectroscopic constants and their predominant configurations. Additionally, Table 5 compiles the bond orders and natural atomic configurations of these states.

The experimentally determined ground state of IrC is the $\Omega = 5/2$ component of $^2\Delta$.[22] In contrast, our calculations indicate that the ground Λ–S state is $[1]^2\Sigma^+$, which aligns with the findings for CoC[54] and the previously discussed RhC. Meanwhile, $[1]^2\Delta$ represents the first excited Λ–S state, exhibiting a quasi-degenerate excitation energy of approximately 1300 cm^{-1}. The literature suggests that DFT identifies $^2\Sigma^+$

as the ground state,[34] while MRCI points to $^2\Delta$.[32] However, our MRCI results still support the $^2\Sigma^+$ state, which may be attributed to the larger basis set employed in our calculations. It is not unusual to find such discrepancies, as SOC can induce inconsistencies between the Λ–S and Ω ground states. For example, a recent theoretical study of the OsO molecule[61] revealed that its Λ–S ground state is $^1\Sigma^+$; the correct Ω ground state $^3\Pi_2$ is achieved only after accounting for SOC. The dominant configurations of the $[1]^2\Sigma^+$ and $[1]^2\Delta$ states are identified as $1\sigma^2 2\sigma^2 3\sigma^1 1\pi^4 1\delta^4$, which has a 75% contribution, and $1\sigma^2 2\sigma^2 3\sigma^2 1\pi^4 1\delta^3$, contributing 80%, respectively. This observation highlights that both states largely exhibit a single-configurational character, while also displaying some multi-configurational traits. Additionally, NBO analysis reveals that in the $[1]^2\Sigma^+$ state the atomic configurations are $6s^{0.89}5d^{7.95}6p^{0.06}$ for iridium and $2s^{1.84}2p^{2.19}$ for carbon. This indicates that the carbon atom is in the ground level ^{3}P, while the iridium atom resides in the first excited state b^{4}F ($5d^8 6s$).[55] In contrast, in the $[1]^2\Delta$ state, the atomic configurations are Ir $6s^{1.57}5d^{7.33}6p^{0.09}$ and C $2s^{1.85}2p^{2.09}$, with the iridium atom represented as a half-and-half mixture of the ground level a^{4}F ($5d^7 6s^2$) and the first excited level b^{4}F.[55]

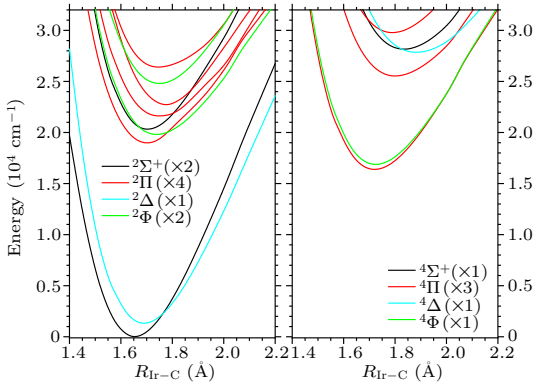


Fig. 3. PECs of low-lying Λ–S states of IrC.

Table 4. Spectroscopic constants of Λ–S states of ^{193}Ir^{12}C.

Λ–S state	T_e (cm^{-1})	R_e (Å)	ω_e (cm^{-1})	B_e (cm^{-1})	Dominant configurations at R_e's $1\sigma/2\sigma/3\sigma/4\sigma/1\pi/2\pi/1\delta$ ($\geq$ 10%) [a]
$[1]^2\Sigma^+$	0	1.652	1214	0.5432	2210404 (75)
$[2]^2\Sigma^+$	20349	1.703	1032	0.5143	2120404 (62)
$[1]^2\Pi$	18978	1.702	1034	0.5153	2210413 (42) + 2200414 (16)
$[2]^2\Pi$	21630	1.747	810	0.4846	2210413 (35) + 2200414 (20) + 2220304 (18)
$[3]^2\Pi$	22724	1.776	1001	0.4730	2210413 (37) + 2220412 (16) + 2200414 (11)
$[4]^2\Pi$	26398	1.748	781	0.4883	2210413 (30) + 2220412 (29) + 2200414 (18)
$[1]^2\Delta$	1314	1.689	1089	0.5192	2220403 (80)
Expt. [b]	0	1.683	1060	0.5268	
$[1]^2\Phi$	19814	1.739	894	0.4890	2210413 (75)
$[2]^2\Phi$	24799	1.751	891	0.4865	2210413 (66) + 2120413 (12)
$[1]^4\Sigma^+$	28087	1.838	822	0.4416	2210314 (69)
$[1]^4\Pi$	16385	1.720	969	0.5007	2210413 (78)
$[2]^4\Pi$	25544	1.806	801	0.4577	2220412 (70)
$[3]^4\Pi$	29803	1.795	795	0.4632	2120413 (51) + 2110414 (17)
$[1]^4\Delta$	27815	1.883	745	0.4177	2220313 (73)
$[1]^4\Phi$	16880	1.724	950	0.4981	2210413 (83)

[a] Computed at the PM-CASSCF level. 1σ and 2σ: C 2s + Ir $5d_\sigma$, 3σ and 4σ: C $2p_\sigma$ + Ir 6s, 1π and 2π: C $2p_\pi$ + Ir $5d_\pi$, and 1δ: Ir $5d_\delta$. The higher-lying three auxiliary active orbitals 5σ and 3π are always weakly occupied.
[b] Ref. [22].

Table 5. Bond orders and natural atomic configurations for Λ–S states of IrC at 1.68 Å.

Λ–S state	MBO	WBI	Atomic config. (Ir)	Atomic config. (C)
$[1]^2\Sigma^+$	2.40	2.23	$6s^{0.89}5d^{7.95}6p^{0.06}$	$2s^{1.84}2p^{2.19}$
$[2]^2\Sigma^+$	2.26	2.19	$6s^{1.50}5d^{7.54}6p^{0.10}$	$2s^{1.52}2p^{2.28}$
$[1]^2\Pi$	1.87	1.65	$6s^{0.78}5d^{7.68}6p^{0.19}$	$2s^{1.84}2p^{2.44}$
$[2]^2\Pi$	1.84	1.64	$6s^{0.94}5d^{7.67}6p^{0.16}$	$2s^{1.75}2p^{2.41}$
$[3]^2\Pi$	1.78	1.58	$6s^{1.35}5d^{7.40}6p^{0.12}$	$2s^{1.82}2p^{2.24}$
$[4]^2\Pi$	1.76	1.53	$6s^{0.79}5d^{7.69}6p^{0.13}$	$2s^{1.84}2p^{2.48}$
$[1]^2\Delta$	2.37	2.13	$6s^{1.57}5d^{7.33}6p^{0.09}$	$2s^{1.85}2p^{2.09}$
$[1]^2\Phi$	1.81	1.58	$6s^{0.97}5d^{7.54}6p^{0.17}$	$2s^{1.78}2p^{2.45}$
$[2]^2\Phi$	1.72	1.50	$6s^{0.97}5d^{7.58}6p^{0.12}$	$2s^{1.78}2p^{2.48}$
$[1]^4\Sigma^+$	1.38	1.20	$6s^{0.90}5d^{7.63}6p^{0.15}$	$2s^{1.83}2p^{2.44}$
$[1]^4\Pi$	1.92	1.68	$6s^{0.92}5d^{7.49}6p^{0.22}$	$2s^{1.83}2p^{2.46}$
$[2]^4\Pi$	1.86	1.57	$6s^{1.52}5d^{7.00}6p^{0.16}$	$2s^{1.81}2p^{2.44}$
$[3]^4\Pi$	1.74	1.59	$6s^{1.20}5d^{7.40}6p^{0.16}$	$2s^{1.59}2p^{2.58}$
$[1]^4\Delta$	1.39	1.16	$6s^{1.45}5d^{7.10}6p^{0.13}$	$2s^{1.85}2p^{2.37}$
$[1]^4\Phi$	1.90	1.66	$6s^{0.89}5d^{7.54}6p^{0.20}$	$2s^{1.83}2p^{2.46}$

For the $[1]^2\Delta$ state, the computed bond length and vibrational frequency are 1.689 Å and 1089 cm^{-1}, respectively, closely aligning with the experimental values of 1.683 Å and 1060 cm^{-1}.[22] The $[1]^2\Sigma^+$ state, which lacks experimental data, exhibits a bond length of 1.652 Å and a vibrational frequency of 1214 cm^{-1}. These results are shorter and higher, respectively, than those of the $[1]^2\Delta$ state, suggesting that the $[1]^2\Sigma^+$ state exhibits stronger bonding characteristics. However, bond order analysis reveals contrasting results. Similar to RhC, the EBO value for the $[1]^2\Sigma^+$ state is 2.5, whereas the $[1]^2\Delta$ state corresponds to a single excitation from the non-bonding 1δ orbital to the bonding 3σ orbital, leading to an increased EBO of 3.0. Consequently, IrC in the $[1]^2\Delta$ state can be approximated as having a triple bond, aligning with the bond order estimated in the literature.[33] Population analysis methods reveal that the bond orders of the $[1]^2\Sigma^+$ and $[1]^2\Delta$ states are quite similar, with MBOs both approximating 2.40, and WBIs at 2.23 and 2.13, respectively. This suggests that the bond orders for both states should be about 2.5. Interestingly, we observe that the three methods used to estimate bond strength provide qualitatively different outcomes: bond length and force constant ($k \propto \omega_e{}^2 \propto R_e{}^{-x} \propto$ bond strength, according to the generalized Badger rule[62]) indicate that the bond in the $[1]^2\Sigma^+$ state is stronger. In contrast, EBO suggests that the bond in the $[1]^2\Delta$ state is stronger, while both MBO and WBI indicate that the bond strengths are essentially similar. This highlights the complexity of bond strength in transition metal systems and underscores the limitations of various estimation methods, which stem from their differing perspectives.

Aside from the $[1]^2\Sigma^+$ and $[1]^2\Delta$ states, all Λ–S electronic states of IrC are found above 2 eV (approximately 16000 cm^{-1}), as illustrated in Fig. 3. Notably, the MBO and WBI values for the $[2]^2\Sigma^+$ state are similar to those of the first two states, while the bond orders of the remaining states generally decrease by 0.5 to 1.0. At 1.68 Å, we conducted tests on the RMS-CASPT2 calculations excluding the p′ active orbitals. Similar to our findings with RhC, the majority of the vertical excitation energy errors fall within 0.1 eV. However, the $[1]^2\Phi$, $[1]^4\Pi$ and $[1]^4\Phi$ states, which have notable Ir 6p occupation numbers, display greater energy deviations ranging from 0.1 eV to 0.15 eV. Notably, the $[1]^2\Pi$ state shows an overestimation of the vertical energy by 0.22 eV. This again emphasizes the critical influence of the p′ shell in specific states.

Since our current findings do not consider SOC effects, we are unable to correlate these results with the experimental observations of Ω states, and thus will refrain from further discussion on that topic.

3.4. Low-lying Ω states of IrC

The PECs of the Ω states within 32000 cm^{-1} are illustrated in Fig. 4. Table 6 summarizes the fitted spectroscopic constants, the dominant Λ–S components and the $|\mu|^2$ values calculated at a bond length of 1.68 Å. The IrC radical experiences significant second-order SOC effects, which indicates that the Λ–S states previously calculated may be insufficient for constructing a reliable spin–orbit matrix. As a result, only the Ω states below 32000 cm^{-1} are included in this analysis.

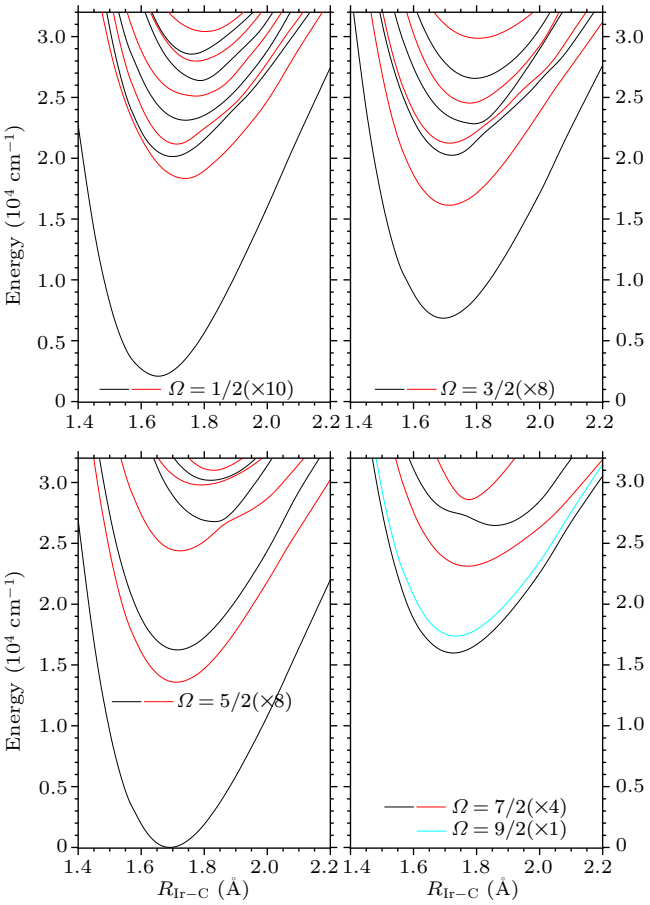


Fig. 4. PECs of low-lying Ω states of IrC.

With the exception of the $X_2{}^2\Delta_{3/2} \leftarrow E_2{}^2\Delta_{3/2}$ emission transition, all identified lower states for the absorption and emission spectral transitions of IrC correspond to the ground state $X_1{}^2\Delta_{5/2}$. The upper states are found within an energy range of 25000 cm^{-1}, with Ω values of 3/2, 5/2 or 7/2.[16,17,22] In the absorption spectra, IrC molecules primarily populate the $v'' = 0$ level of the ground state, although absorption spectra from the $v'' = 1$ level have also been observed at room temperature.[14] Due to the Boltzmann distribution, populations in higher vibrational and electronic states are negligible for this analysis. Based on the Ω quantum numbers, the predominant Λ–S components, the alignment of theoretical and experimental excitation energies and the significant $|\mu|^2$ values, most of these upper states closely match the calculated Ω states. Their corresponding experimental spectroscopic constants are detailed in Table 6 for reference.

Table 6. Spectroscopic constants of Ω states of $^{193}Ir^{12}C$.[a)]

Ω state	T_e (cm^{-1})	R_e (Å)	ω_e (cm^{-1})	B_e (cm^{-1})	$\lvert\mu^2\rvert$ (a.u.)[b)]			Components[b)] ($\geq$ 10%)
					{1}1/2	{1}3/2	{1}5/2	
{1}1/2	2068	1.653	1183	0.5466				$[1]^2\Sigma^+$ (98)
Expt.	x_2 ≈3200	1.682	[1030]	0.5272				$X_2{}^2\Delta_{3/2}$; $X_2{}^2\Sigma^+_{1/2}$ [c)]
{2}1/2	18332	1.740	995	0.4955	0.0406	0.0387		$[1]^4\Pi$ (47) + $[1]^2\Pi$ (31) + $[2]^2\Pi$ (10)
{3}1/2	20134	1.699	1007	0.5136	0.4014	0.1223		$[1]^2\Pi$ (54) + $[1]^4\Pi$ (35)
{4}1/2	21294	1.715	964	0.5074	0.0488	0.0049		$[2]^2\Sigma^+$ (74) + $[2]^2\Pi$ (11)
{5}1/2	23119	1.744	849	0.4905	0.0182			$[1]^4\Pi$ (84)
{6}1/2	25032	1.758	817	0.4826	0.4029	0.0022		$[2]^2\Pi$ (51) + $[3]^2\Pi$ (15) + $[1]^4\Pi$(13)
{7}1/2	26543	1.779	905	0.4713	0.0196	0.1411		$[3]^2\Pi$ (70) + $[2]^2\Pi$ (14)
{8}1/2	27986	1.781	875	0.4706		0.0148		$[2]^4\Pi$ (74)
{9}1/2	28594	1.767	917	0.4779	0.0034	0.0218		$[2]^4\Pi$ (78)
{10}1/2	30397	1.800	797	0.4604	0.1116	0.1454		$[4]^2\Pi$ (58) + $[2]^4\Pi$ (14)
{1}3/2	6846	1.694	1068	0.5161	0.0019		0.0018	$[1]^2\Delta$ (96)
{2}3/2	16130	1.712	976	0.5045	0.0283		0.0120	$[1]^4\Pi$ (89)
Expt.	x_2+12180	1.703	[960]	0.5148				$E_2{}^2\Delta_{3/2}$; $E_2{}^2\Pi_{1/2}$ [c)]
Expt.	[16504]							U_2 [d)]
{3}3/2	20233	1.722	1053	0.5042	0.2084		0.3190	$[1]^2\Pi$ (90)
Expt.	19643	1.720	850	0.5045				$K^2\Pi_{3/2}$ [e)]
{4}3/2	21238	1.715	970	0.5087	0.0005		0.0004	$[1]^4\Phi$ (99)
Expt.	[19435]	[1.714]		[0.5085]				$[19.4]^2\Pi_{3/2}$ [e)]
{5}3/2	22810	1.768	922	0.4773	0.0864	0.0007	0.0452	$[2]^2\Pi$ (79) + $[3]^2\Pi$ (10)
Expt.	~22500	~1.78		~0.47				$U_3 3/2$ and $U_4 3/2$ (v' =2 observed) [e)]
{6}3/2	24536	1.775	868	0.4734	0.2243		0.1209	$[3]^2\Pi$ (79)
Expt.	23420	1.766	829	0.4782				$[23.0]^2\Pi_{3/2}$ [e)]
{7}3/2	26502	1.805	848	0.4582	0.1911		0.0221	$[2]^4\Pi$ (59) + $[4]^2\Pi$ (35)
{8}3/2	29886	1.803	657	0.4589	0.1462		0.0038	$[3]^4\Pi$ (39) + $[4]^2\Pi$ (23) + $[2]^4\Pi$ (13)
{1}5/2	0	1.691	1082	0.5184				$[1]^2\Delta$ (99)
Expt.	0	1.683	1060	0.5268				$X_1{}^2\Delta_{5/2}$
{2}5/2	13581	1.711	998	0.5064			0.0006	$[1]^4\Pi$ (98)
Expt.	15149	1.705	964	0.5132				$E_1{}^2\Delta_{5/2}$; $E_1{}^4\Pi_{5/2}$ [c)]
Expt.	[15846]							U_1 [d)]
{3}5/2	16236	1.714	985	0.5046		0.0028	0.0002	$[1]^4\Phi$ (55) + $[1]^2\Phi$ (43)
{4}5/2	24376	1.723	962	0.5005		0.0068		$[1]^2\Phi$ (47) + $[1]^4\Phi$ (42) + $[2]^2\Phi$ (10)
{5}5/2	26731	1.816	985	0.4525		0.0052		$[2]^4\Pi$ (62) + $[3]^4\Pi$ (22) + $[1]^4\Delta$ (14)
{6}5/2	29791	1.788	640	0.4666		0.4693	0.0003	$[2]^2\Phi$ (85)
{7}5/2	30085	1.829	804	0.4461				$[3]^4\Pi$ (75) + $[2]^4\Pi$ (23)
{8}5/2	30802	1.826	999	0.4474		0.0097		$[1]^4\Delta$ (84) + $[2]^4\Pi$ (12)
{1}7/2	15984	1.726	930	0.4977			0.0406	$[1]^4\Phi$ (70) + $[1]^2\Phi$ (28)
Expt.	14414	1.718	936	0.5053				$D^2\Phi_{7/2}$; $D(^4\Phi +^2\Phi)_{7/2}$ [c)]
Expt.	[15278]	[1.722]	[924]	[0.5034]				$D^2\Phi_{7/2}$ [e)]
{2}7/2	23125	1.772	789	0.4704			0.3642	$[2]^2\Phi$ (53) + $[1]^2\Phi$ (25) + $[1]^4\Phi$ (20)
Expt.	20930	1.756	833	0.4841				$L^2\Phi_{7/2}$ [f)]
{3}7/2	26622	1.861	569	0.4311			0.0866	$[1]^2\Phi$ (46) + $[2]^2\Phi$ (38)
{4}7/2	28561	1.775	1399	0.4665			0.0137	$[1]^4\Delta$ (92)
{1}9/2	17375	1.734	921	0.4925				$[1]^4\Phi$ (99)

[a)]Experimental spectroscopic constants are taken from Reference [22] by default. The values in brackets are T_0, R_0, $\Delta G_{1/2}$ and B_0. State U_n means the nth unrecognized state in the literature.
[b)]Computed at 1.68 Å. [c)]Ref. [32]. [d)]Ref. [14]. [e)]Ref. [17]. [f)]Ref. [16].

The lowest three Ω states from $[1]^2\Sigma^+$ and $[1]^2\Delta$ The SOC effects result in the splitting of the $[1]^2\Delta$ state into two Ω sub-states, namely {1}3/2 and {1}5/2. In contrast, the $[1]^2\Sigma^+$ state remains unsplit, comprising solely the {1}1/2 state with minimal second-order SOC contributions from other Λ–S states. Among the three Ω states, {1}5/2 is identified as the ground state, aligning with the experimental ground state $X_1{}^2\Delta_{5/2}$ (or $X_1 5/2$)[22] and the theoretical one by Balasubramanian *et al.*[32] Meanwhile, {1}1/2 and {1}3/2 correspond to the first and second excited states, with energies near 2000 and 6800 cm^{-1}, respectively. Additionally, experimental findings have reported a state referred to as $X_2{}^2\Delta_{3/2}$ (or $X_2 3/2$) during the $E_2 3/2 \rightarrow X_2$ transition.[14] This state was thought to represent the $\Omega = 3/2$ sub-state of the $[1]^2\Delta$ state; how-

ever, its estimated energy of approximately 3200 cm^{-1} is significantly lower than the theoretical energy predicted for the $\{1\}3/2$ state, being 6846 cm^{-1} in this study or 6506 cm^{-1} in the work by Balasubramanian *et al.*[32] Due to this reason, Balasubramanian *et al.* redefined this state as $X_2{}^2\Sigma^+_{1/2}$.[32] We have thoroughly analyzed two potential scenarios: (I) If we consider the $\Omega = 3/2$ state as initially labeled,[14] the experimentally observed transition $E_2 3/2 \rightarrow X_2$ (which corresponds to $\{2\}3/2 \rightarrow \{1\}3/2$ or $\{3\}3/2 \rightarrow \{1\}3/2$ in this research) would be nearly forbidden, given its tiny $|\mu|^2$ value. (II) If we reclassify it as the $\Omega = 1/2$ state, as suggested by Balasubramanian *et al.*,[14] the $|\mu|^2$ value for the $E_2 3/2 \rightarrow X_2$ transition (which can only correlate to $\{2\}3/2 \rightarrow \{1\}1/2$ at this stage) is approximately 0.03 a.u., indicating a transition of moderate strength. Thus, it is logical to redefine this state as $X_2{}^2\Sigma^+_{1/2}$ (or simply $X_2 1/2$), which has been adopted in this study. The theoretical bond length for the $X_1{}^2\Delta_{5/2}$ state is determined to be 1.691 Å, with a vibrational frequency of 1082 cm^{-1}, closely matching the experimental values of 1.683 Å and 1060 cm^{-1}, respectively. For the $X_2{}^2\Sigma^+_{1/2}$ state, the experimental excitation energy of 3200 cm^{-1} is close to the theoretical value of 3406 cm^{-1} calculated by Balasubramanian *et al.*[32] but is significantly larger than the value of 2068 cm^{-1} in this study, indicating that the theoretical energy of the $[1]^2\Sigma^+$ state might be underestimated by about 1000 cm^{-1}. Additionally, a notable discrepancy also exists between the other theoretical and experimental spectroscopic constants of this state. It is crucial to highlight that these experimental values were derived under the assumption that both the $X_1 5/2$ and $X_2 3/2$ states originate from $^2\Delta$.[14] Consequently, future experiments should re-evaluate these measurements.

The $D^2\Phi_{7/2}$ state The $D^2\Phi_{7/2}$ state observed in experiments[14,15,17] corresponds to our calculated $\{1\}7/2$ state. Notably, its primary Λ–S component is $^4\Phi$, while the $^2\Phi$ component plays a minor role. Balasubramanian *et al.* reached similar conclusions, leading them to propose renaming this state as $D(^4\Phi + {}^2\Phi)_{7/2}$.[32] Our calculated excitation energy of 15984 cm^{-1} is considerably higher than the earlier experimental figure of 14414 cm^{-1},[14] yet it aligns more closely with later measurements of approximately 15100 cm^{-1}[15] and around 15300 cm^{-1},[17] while the theoretical energy of 13719 cm^{-1} by Balasubramanian *et al.*[32] seems too low. Additionally, the calculated equilibrium bond length of 1.726 Å and vibrational frequency of 930 cm^{-1} are in strong agreement with the experimental values of 1.718 Å and 936 cm^{-1},[22] respectively.

The $E_1{}^2\Delta_{5/2}$ and $E_2{}^2\Delta_{3/2}$ states In the two weak band systems $E_1 \leftrightarrow X_1$ and $E_2 \rightarrow X_2$, the upper states have been associated with the Ω sub-states of the parent state $E^2\Delta$ lying at about 15000 cm^{-1}. However, as illustrated in Fig. 3, this $^2\Delta$ state is not observed in our calculations below an energy of 32000 cm^{-1}. Balasubramanian *et al.*[32] reclassified these two states as $E_1{}^4\Pi_{5/2}$ and $E_2{}^2\Pi_{1/2}$, respectively, although the latter was hypothesized at a lower theoretical level. In this study, we identify E_1 as the $\{2\}5/2$ state, primarily corresponding to the $\Omega = 5/2$ sub-state of $[1]^4\Pi$, while the calculated energy of 13581 cm^{-1} is smaller than the experimental value of 15149 cm^{-1}[22] and the theoretical value of 14968 cm^{-1} by Balasubramanian *et al.*[32] The energy of the E_2 state, being about 15500 cm^{-1}, is significantly lower than that of the $\{3\}3/2$ state, although its dominant component is $[1]^2\Pi$; hence, it is categorized as the $\{2\}3/2$ state lying at 16130 cm^{-1}, which fundamentally represents the $\Omega = 3/2$ sub-state of $[1]^4\Pi$. Table 6 shows that the bond lengths for the $\{2\}5/2$ and $\{2\}3/2$ states are approximately 1.71 Å, differing by less than 0.01 Å from the experimental values. Additionally, the vibrational frequencies align well with the experimental data. At room temperature, two absorption peaks were identified at 15846 cm^{-1} and 16504 cm^{-1},[14] referred to as the U_1 and U_2 states in this study. While no definitive assignments have been made, these peaks are hypothesized to correspond to the absorption band systems of $X_1 \rightarrow E_1$ and E_2, suggesting a potential association with the $\{2\}5/2$ and $\{2\}3/2$ states, respectively.

The $K^2\Pi_{3/2}$ and $[19.4]^2\Pi_{3/2}$ states The experimentally observed $K^2\Pi_{3/2}$ and $[19.4]^2\Pi_{3/2}$ states are very close in energy, both around 19500 cm^{-1}.[14,17] However, among the calculated $\Omega = 3/2$ states near this energy, only the leading component of the $\{3\}3/2$ state is $^2\Pi$. The $|\mu|^2$ value of approximately 0.32 a.u. between $\{3\}3/2$ and the ground state is rather large, indicating a strong transition. Therefore, $\{3\}3/2$ should correspond to the $K^2\Pi_{3/2}$ state. Additionally, there exists another Ω state, $\{4\}3/2$, derived from $[1]^4\Phi$, which has a similar energy but a very small $|\mu|^2$ value to the ground state. Given that the $[19.4]^2\Pi_{3/2} \rightarrow X_1{}^2\Delta_{5/2}$ transition has been experimentally identified as weak,[17] the upper state $[19.4]^2\Pi_{3/2}$ could be associated with the calculated $\{4\}3/2$ state. The theoretical bond lengths for both the $K^2\Pi_{3/2}$ and $[19.4]^2\Pi_{3/2}$ states align well with experimental data; however, the theoretical vibrational frequency for the $K^2\Pi_{3/2}$ state is 200 cm^{-1} greater than the experimental value.

The $L^2\Phi_{7/2}$ state The $L^2\Phi_{7/2}$ state observed in experiments[14,16] aligns with the calculated $\{2\}7/2$ state, and its primary component, $[1]^2\Phi$, aligns with experimental expectations. Furthermore, the theoretically predicted bond length and vibrational frequency are generally consistent with experimental values, although the excitation energy of 23125 cm^{-1} is about 2200 cm^{-1} higher than the experimental value of approximately 20930 cm^{-1}. In experiments, the $L^2\Phi_{7/2} \rightarrow X_1{}^2\Delta_{5/2}$ transition exhibits notable strength,[16] as evidenced by the calculated $|\mu|^2$ value of approximately 0.36 a.u.

The $[23.0]^2\Pi_{3/2}$ state Pang and Cheung[17] identified the

$[23.0]^2\Pi_{3/2}$ state at an energy of approximately 23400 cm^{-1}. Given its dominant Λ–S component and excitation energy, this state can be confidently assigned to the calculated $\{6\}3/2$ state, which arises mainly from $[3]^2\Pi$. The theoretical values of T_e and R_e align well with the experimental data, though the vibrational frequency is computed to be 39 cm^{-1} higher than that observed in experiments.

Preliminary assignment to other spectral bands Using theoretical results, we can analyze the unassigned absorption transitions observed in experiments. Specifically, the U_1 and U_2 states[14] have been aligned with the $E_1{}^4\Pi_{5/2}$ and $E_2{}^4\Pi_{3/2}$ states, or the calculated $\{2\}5/2$ and $\{2\}3/2$ states. Moreover, Pang and Cheung[17] identified two absorption transitions at energies of 23937 cm^{-1} and 24313 cm^{-1}, with the total angular momentum quantum numbers and vibrational quantum numbers of the unclassified upper states both being $\Omega = 3/2$ and $v' = 2$. In this paper, these two states are denoted as $U_3 3/2$ and $U_4 3/2$, respectively. Considering that the vibrational frequencies of most Ω states of IrC fall within the range of 800 cm^{-1} to 1000 cm^{-1} (as indicated in Table 6), if the identified vibrational levels are accurate, the adiabatic excitation energies for the two states at $v' = 0$ are expected to be approximately 22000 cm^{-1} and 22500 cm^{-1}, closely aligning with the energy of the $\{5\}3/2$ state. Given the limited experimental data available, we tentatively propose that these two transitions correspond to the $\{5\}3/2$ state, which primarily originates from the $[2]^2\Pi$ state, exhibiting a notable $|\mu|^2$ value of around 0.045 a.u. Further experimental investigations will be necessary to verify this assumption in the future.

4. Conclusion

The presence of open-shell d orbitals and notable SOC effects complicates the spectral analysis of transition metal compounds, requiring highly precise calculations. In experimental studies, numerous spectral transitions of RhC and IrC have been detected and analyzed. However, some of the electronic states identified in these experiments do not align with the earlier theoretical findings by Balasubramanian *et al.* published in 1997.[25,32]

In this paper, we utilize the RMS-CASPT2 method in conjunction with the SI approach to systematically compute the PECs of the low-lying Λ–S and Ω states of RhC and IrC radicals, spanning up to 32000 cm^{-1}. Additionally, we fit the spectroscopic constants associated with these states. For the Λ–S states, we conduct an analysis of their bond orders and atomic configurations. Drawing on our theoretical findings for the Ω states, we have successfully assigned the experimentally observed states of RhC and IrC to their corresponding calculated states. Notably, the theoretical spectroscopic constants align closely with the experimental values. This research serves as a valuable reference for future spectroscopic studies of RhC and IrC.

Supplement After the acceptance of this manuscript, Tomchak and Morse[63] published the dissociation energies of RhC and IrC using resonant three-photon ionization spectroscopy.

Acknowledgements

Project supported by the National Natural Science Foundation of China (Grant Nos. 22073072 and 12274178) and the Double First-Class University Construction Project of Northwest University.

References

[1] Tian D, Denny S R, Li K, Wang H, Kattel S and Chen J G 2021 *Chem. Soc. Rev.* **50** 12338
[2] Ma X, Ge Y, Hou Y, Shi K, Zhang J, Yue G, Tao Q and Zhu P 2025 *Chin. Phys. B* **34** 086104
[3] Bannikov V V, Shein I R and Ivanovskii A L 2009 *Phys. Status Solidi RRL* **3** 218
[4] Zhao Z, Xu L, Wang M, Cui L, Wang L M, He J, Liu Z and Tian Y 2010 *Phys. Status Solidi RRL* **4** 230
[5] Lagerqvist A, Neuhaus H and Scullman R 1965 *Zeitschrift für Naturforschung* **20a** 751
[6] Lagerqvist A and Scullman R 1966 *Arkiv för Fysik* **32** 479
[7] Korwar V M 1967 *Proc. Phys. Soc.* **92** 523
[8] Kaving B and Scullman R 1969 *J. Mol. Spectrosc.* **32** 475
[9] Brom Jr. J M, Graham W R M and Weltner Jr. W 1972 *J. Chem. Phys.* **57** 4116
[10] Li X and Wang L S 1998 *J. Chem. Phys.* **109** 5264
[11] Balfour W J, Fougère S G, Heuff R F, Qian C X W and Zhou C 1999 *J. Mol. Spectrosc.* **198** 393
[12] Gong Y, Andrews L, Gonçalves A P, Pereira C C L and Marçalo J 2012 *Chem. Phys. Lett.* **528** 7
[13] Jansson K, Scullman R and Yttermo B 1969 *Chem. Phys. Lett.* **4** 188
[14] Jansson K and Scullman R 1970 *J. Mol. Spectrosc.* **36** 248
[15] Marr A J, Flores M E and Steimle T C 1996 *J. Chem. Phys.* **104** 8183
[16] Ma T, Leung J W H and Cheung A S C 2004 *Chem. Phys. Lett.* **385** 259
[17] Pang H F and Cheung A S C 2009 *Chem. Phys. Lett.* **471** 194
[18] Auwera-Mahieu A V and Drowart J 1967 *Chem. Phys. Lett.* **1** 311
[19] McIntyre N S, Auwera-Mahieu A V and Drowart J 1968 *Trans. Faraday Soc.* **64** 3006
[20] Tomchak K H and Morse M D 2025 *J. Phys. Chem. A* **129** 8563
[21] Merriles D M, Barrera-Casas Y, Knapp A S and Morse M D 2024 *J. Chem. Phys.* **160** 084303
[22] Huber K P and Herzberg G 1979 *Molecular Spectra and Molecular Structure, volume IV. Constants of Diatomic Molecules* (New York: Van Nostrand Reinhold)
[23] Shim I and Gingerich K A 1984 *J. Chem. Phys.* **81** 5937
[24] Mains G J and White J M 1991 *J. Phys. Chem.* **95** 112
[25] Tan H, Liao M and Balasubramanian K 1997 *Chem. Phys. Lett.* **280** 423
[26] Stevens F, Van Speybroeck V, Carmichael I, Callens F and Waroquier M 2006 *Chem. Phys. Lett.* **421** 281
[27] Wang J, Sun X and Wu Z 2006 *Chem. Phys. Lett.* **426** 141
[28] Jia L C, Zhao R N, Han J G, Sheng L S and Cai W P 2008 *J. Phys. Chem. A* **112** 4375
[29] Kharat B, Deshmukh S B and Chaudhari A 2009 *Int. J. Quantum Chem.* **109** 1103
[30] Jensen K P 2009 *J. Phys. Chem. A* **113** 10133
[31] Wang J, Manivasagam S and Wilson A K 2015 *J. Chem. Theory Comput.* **11** 5865
[32] Tan H, Liao M and Balasubramanian K 1997 *Chem. Phys. Lett.* **280** 219
[33] Xie X G, Bi X J, Cao H and Dai S S 1998 *Chin. Chem. Lett.* **9** 1133
[34] Wang J, Sun X and Wu Z 2007 *J. Clust. Sci.* **18** 333
[35] Liu W and Peng D 2009 *J. Chem. Phys.* **131** 031104

[36] Peng D and Reiher M 2012 *Theor. Chem. Acc.* **131** 1081
[37] Zobel J P, Widmark P O and Veryazov V 2020 *J. Chem. Theory Comput.* **16** 278
[38] Zobel J P, Widmark P O and Veryazov V 2021 *J. Chem. Theory Comput.* **17** 3233
[39] Andersson K, Malmqvist P A, Roos B O, Sadlej A J and Wolinski K 1990 *J. Phys. Chem.* **94** 5483
[40] Andersson K, Malmqvist P A and Roos B O 1992 *J. Chem. Phys.* **96** 1218
[41] Ghigo G, Roos B O and Malmqvist P Å 2004 *Chem. Phys. Lett.* **396** 142
[42] Battaglia S, Fransén L, Galván I F and Lindh R 2022 *J. Chem. Theory Comput.* **18** 4814
[43] Battaglia S and Lindh R 2021 *J. Chem. Phys.* **154** 034102
[44] Malmqvist P Å and Roos B O 1989 *Chem. Phys. Lett.* **155** 189
[45] Schimmelpfennig B 1996 *AMFI: atomic mean field integral program* (University of Stockholm, Stockholm, Sweden)
[46] Zhang Y, Suo B, Wang Z, Zhang N, Li Z, Lei Y, Zou W, Gao J, Peng D, Pu Z, Xiao Y, Sun Q, Wang F, Ma Y, Wang X, Guo Y and Liu W 2020 *J. Chem. Phys.* **152** 064113
[47] Fdez Galván I, Vacher M, Alavi A, *et. al.* 2019 *J. Chem. Theory Comput.* **15** 5925
[48] Aquilante F, Autschbach J, Baiardi A, *et. al.* 2020 *J. Chem. Phys.* **152** 214117
[49] Li C and Zou W 2026 *Chem. Phys. Lett.* **882** 142454
[50] Le Roy R J 2017 *J. Quant. Spectrosc. Radiat. Transf.* **186** 167
[51] Lu T and Chen F 2012 *J. Comput. Chem.* **33** 580
[52] Lu T 2024 *J. Chem. Phys.* **161** 082503
[53] Glendening E D, Badenhoop J K, Reed A E, Carpenter J E, Bohmann J A, Morales C M, Landis C R and Weinhold F 2013 *NBO version 6.0* (Theoretical Chemistry Institute, University of Wisconsin, Madison, WI)
[54] Tzeli D and Mavridis A 2006 *J. Phys. Chem. A* **110** 8952
[55] Kramida A, Ralchenko Y, Reader J and Team N A Dec. 2024 *NIST Atomic Spectra Database* (version 5.12) (Gaithersburg: National Institute of Standards and Technology)
[56] Xiao L, Yang Y, Zou W and Yan B 2025 *Mol. Phys.* **123** e2361116
[57] Peterson K A, Figgen D, Dolg M and Stoll H 2007 *J. Chem. Phys.* **126** 124101
[58] Kendall R A, Dunning T H and Harrison R J 1992 *J. Chem. Phys.* **96** 6796
[59] Zou W and Suo B 2016 *J. Phys. Chem. A* **120** 6357
[60] Fougère S G 2000 *The Electronic Structure and Spectroscopy of Rhodium Diatomic Molecules* (PhD Dissertation, British Columbia: University of Victoria). p. 116
[61] Yan W and Zou W 2023 *Chin. Phys. B* **32** 113101
[62] Kraka E, Larsson J A and Cremer D 2010 *Computational Spectroscopy* Ed. by Grunenberg J (New York: Wiley) pp. 105–149
[63] Tomchak K H and Morse M D 2025 *J. Phys. Chem. A* **129** 8563